Characterization of $TaSi_2$–Si composites for use as wide-bandpass optical elements for synchrotron radiation

S. R. Stock[a)]
School of Materials Science and Engineering, Georgia Institute of Technology, Atlanta, Georgia 30332-0245

Z. U. Rek
Stanford Synchrotron Radiation Laboratory, P. O. Box 4349, Bin 69, Stanford, California 94309-0210

M. S. Goorsky
Department of Materials Science and Engineering, University of California Los Angeles, Los Angeles, California 90024-1595

(Received 28 September 1995; accepted for publication 16 January 1996)

The wide rocking curves of matrix reflections of the *in situ* eutectic composite $TaSi_2$–Si make wafers of this material attractive for use as wide-bandpass monochromators for synchrotron radiation, and characterization of wafers of $TaSi_2$–Si for use with energies normally accessible at storage rings (i.e., 5–40 keV) is the focus of the present report. A wafer with $[111]_{Si}$ orientation and a wafer with $[110]_{Si}$ orientation are studied. The high degree of preferred orientation of the $TaSi_2$ rods relative to the Si matrix is examined using synchrotron Laue patterns, and the 100_{TaSi_2}, 003_{TaSi_2}, 101_{TaSi_2}, and 102_{TaSi_2} reflections are used to establish the orientation relationship and to determine that the spread of rod orientations is at least 5° and probably no greater than 6°. Double-axis diffractometry with Cu $K\alpha$ radiation reveals matrix reflections with rocking curve widths that are about 20 times broader than those from perfect Si and with peak reflectivities approaching 20%. The rocking curves widths are found to be relatively insensitive to irradiated area, thus indicating that most of the observed width is not due to long-range bending. Triple-axis diffractometry with Cu $K\alpha$ radiation reveals that considerable compressive strain exists in the matrix and that much of the width of the diffraction peak is due to mosaicity. The performance of the $[111]_{Si}$ $TaSi_2$–Si wafer and a perfect [111] Si wafer as monochromators for microradiography are compared, and a gain of an order of magnitude in x-ray intensity delivered to the sample is demonstrated with the composite crystal. © *1996 American Institute of Physics.* [S0021-8979(96)00909-1]

INTRODUCTION

Directional solidification of semiconductor–metal eutectic mixtures commonly yields aligned arrays of metallic rods in a single-crystal semiconductor matrix,[1–7] and the *in situ*, three-dimensional array of rectifying junctions offers interesting electronic properties.[8] The Si–$TaSi_2$ composites are the most promising of these systems, and considerable electronic and microstructural data has been gathered.[8–10] Synchrotron white beam topography of $\langle 111\rangle_{Si}$-oriented Si–$TaSi_2$ wafers has shown that the $TaSi_2$ rods are highly oriented with respect to the Si matrix, projection topographs have revealed little substructure, and x-ray double-axis diffractometry has found rocking curves approximately 20 times broader than those from perfect Si crystals.[11]

The widths of the Si rocking curve in $TaSi_2$–Si suggest that these composites may be good wide-bandpass monochromators for synchrotron radiation, and the present report examines this proposition. The goal of a wide-bandpass monochromator is to produce higher intensities than perfect crystals of Si or Ge, and multilayers or even mosaic crystals are optical elements allowing one to use the entire divergence of the beam.[12] Approaches to increasing bandpass include mechanical lapping of Si wafers[13] and annealing of Si crystals to produce oxygen precipitates,[14] and, as is discussed below, the $TaSi_2$–Si composite appears to be a very attractive alternative.

In this work double-axis diffractometry is used to examine the role of long-range bending on rocking curve widths; results from $[111]_{Si}$ and $[\bar{1}01]_{Si}$-oriented $TaSi_2$–Si composite wafers are also compared. Triple-axis diffractometry is used to map reciprocal space around the 111 and 333 Bragg peaks for the $[111]_{Si}$ wafer. Synchrotron transmission Laue patterns of the $[111]_{Si}$ and $[\bar{1}01]_{Si}$ wafers are used to investigate the orientation relationships between Si matrix and $TaSi_2$ rods, following the earlier approach used to characterize the texture of the rods relative to the matrix.[11] Laboratory $\theta/2\theta$ diffractometry provides a confirmation that little, if any, of the $TaSi_2$ phase is oriented in other than the predominant highly defined texture.

BACKGROUND

The Si–$TaSi_2$ semiconductor–metal composites are grown by directional solidification of the eutectic composition, and the highly perfect Si matrix contains several vol % of the metallic $TaSi_2$ in the form of rods oriented parallel to the $[111]_{Si}$ growth direction. Typically, there are about $1–2\times10^6$ rods/cm^2 with an average rod diameter of about 1 μm and an average inter-rod spacing of about 8 μm.[9] Clusters of dislocations (with densities approaching 10^7 cm^{-2}) have been observed with transmission electron microscopy

a)Electronic mail: stuart.stock@mse.gatech.edu

 0021-8979/96/79(9)/6803/8/$10.00

(TEM) in some regions of the sample,[15] and the results of double-axis diffractometry are consistent with these densities.[11]

Synchrotron transmission Laue patterns exploit the continuous spectrum of nearly parallel x radiation emitted from bending magnets or wigglers; each Bragg spot is a map of the variation of diffracting power within the volume of material irradiated by the beam. In the case of the $TaSi_2$–Si composite system, both the Si matrix and the $TaSi_2$ rods (more precisely each individual rod) produce diffracted intensity within the Laue pattern.[11] As each diffraction plane selects a wavelength satisfying the Bragg equation, the single-crystal Si matrix produces an array of sharply defined spots while the array of slightly misoriented $TaSi_2$ rods produces what appears at low magnification to be diffuse streaks. The method used for verifying that the streaks are from diffraction from $TaSi_2$ involves recording the Laue pattern with and without filters (in the beam) possessing absorption edges in the wavelength range expected in the streaks. The images of rods diffracting wavelengths higher than that of the absorption edge suffer relatively little attenuation while the images produced with wavelengths just below the edge are essentially eliminated. The resulting sharp change in contrast allows precise determination of d spacings.[11]

X-ray double-axis diffractometry is widely used to assess crystalline quality of a range of single crystals. Double-axis rocking curve widths are determined primarily by the excess dislocation density, i.e., by the shear strains or the range of misorientations, in the specimen area irradiated and not by the dilational strains. In order to isolate the dilational strains one must perform a high-resolution $\theta/2\theta$ scan with a very narrow detector "slit," which is, in practice, a post-sample analyzer crystal oriented to rediffract x rays diffracted from the sample (i.e., triple-axis diffractometry). Varying the orientation of the analyzer crystal slightly from the exact Bragg position and scanning the sample crystal through its range of reflection allows one to map reciprocal space in the vicinity of the sample's Bragg peak. Separation of the dilational strain and mosaicity by triple-axis diffractometry, is, therefore, quite valuable to understanding the origin of the broad rocking curve widths in $TaSi_2$–Si composites and to assessing the degree to which these crystals will be able to function as wide-bandpass optical elements for synchrotron radiation.

EXPERIMENTAL METHODS

The growth axis for the two wafers discussed in this article is $[111]_{Si}$. One wafer was cut from a boule so that its face is perpendicular to the growth direction, i.e., the face is $(111)_{Si}$ and the $TaSi_2$ rods are perpendicular to the surface. The second wafer is a longitudinal $(\bar{1}01)_{Si}$ section of a boule. The $[111]_{Si}$ growth direction is in the plane of the wafer and the $TaSi_2$ rods are parallel to the surface. Both wafers were polished with colloidal silica, and the thicknesses of the $[111]_{Si}$ wafer is 0.5 mm and that of the $[\bar{1}01]_{Si}$ wafer is about 1.0 mm.

Powder diffractometry (Philips PW1800, $\theta/2\theta$ geometry) of the two wafers was used to confirm the Si matrix orientation and to reveal evidence of the orientation of the $TaSi_2$ phase relative to the Si matrix. The diffractometer was equipped with a copper target and operated at 40 kV and 30 mA; an area of 10×10 mm^2 was irradiated. As the object of the scans was to confirm the orientations of $TaSi_2$ present, the scans were run rapidly from 10° to 85° or 115° 2θ with a step size of 0.05° 2θ and counting time of 0.5 s/step.

Synchrotron Laue patterns were recorded on Beam Line 2-2 of SSRL using a 1-mm-diam collimator with and without a 75-μm-thick Mo filter. The 1 mm collimated beam then passed through lead shielding positioned to minimize scatter reaching the sample. After passing through the sample, the polychromatic beam was intercepted, prior to reaching the film, by a cup-shaped beam stop attached to the film holder. In a small number of cases the beam stop was not used so that the position of the beam could be very precisely fixed: Even though the film was fogged for some distance around the position where the beam hit the film, the 1 mm footprint of the beam could be discerned under oblique lighting. A 1-mm-thick Al plate was used to cover the film in order to control the amount scatter contributed to the darkening of the film.

The specifics of the goniometer used to record the Laue patterns are presented elsewhere,[11] and the sample-to-film separations were set using a linear translation table. Note that the translation axis was measured to be within 0.1° of parallel to the x-ray beam axis in both the horizontal and vertical directions. At least three film-to-sample separations were used for each $TaSi_2$ reflection used, the minimum separation between the film positions was 30.0 mm, and the separations were set to a precision of better than 50 μm. Extrapolation of diffracted beams positions to zero film-to-sample distance is necessary to fix the Bragg angle for the absorption edge in the $TaSi_2$ streaks and corresponding d spacing accurately enough to identify the diffracting plane indices.[16] Exposure times were similar to those used before.[11] Kodak SR5 film was used to record the majority of exposures, Polaroid P52 or P57 film was used during sample orientation, and Fuji Image plates (Fuji HR-IIIN) were used to record selected Laue patterns. The two wafers were oriented on the goniometer so that diffraction from the following $TaSi_2$ reflections at the wavelength of the Mo K_{edge} could be observed: 003, 006, 102, 101, and 100. The first three were observed in the $[\bar{1}01]_{Si}$ wafer, and the last two in the $[111]_{Si}$ wafer.

Reflection topographs were recorded of the $[\bar{1}01]_{Si}$ wafer using polychromatic radiation and were of interest because of the anisotropy of the contrast in the topographs: Earlier transmission and reflection topographs with polychromatic radiation of the $[111]_{Si}$ wafer showed few features of interest.[11] The wafer was aligned so that the x-ray beam was incident at an angle approximately 22° from the surface. Two reflection Laue patterns were recorded, the first with the incident beam coplanar with $[111]_{Si}$ and the second rotated 90° with respect to the first orientation, i.e., with the incident beam coplanar with $[1\bar{2}1]_{Si}$. A 1 mm Al plate was used to reduce the contribution of scatter to the topographs.

Double-axis diffractometry was performed with Cu $K\alpha$ radiation, and scans were recorded at both Georgia Tech and SSRL. The scans from Georgia Tech were recorded on a Bede QC2a system with a 400_{Si} monochromator. The SSRL

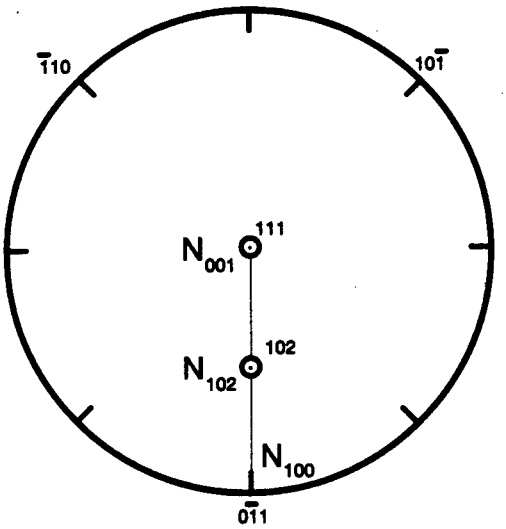

FIG. 1. Stereographic projection show in the relationship between directions in the Si matrix and plane normals in the $TaSi_2$ rods. The directions in the Si matrix are denoted by "*hkl*" while the normals to the $(mn.o)_{TaSi_2}$ are shown as "N_{mno}."

FIG. 2. Laue pattern recorded with the $[\bar{1}01]_{Si}$ wafer oriented so that 003_{TaSi_2} (labeled "1") would diffract a range of wavelengths on either side of the Mo *K* edge. The position of the beam stop is indicated by "O."

double-axis diffractometer used a 333_{Si} monochromator reflection from a $\langle 110\rangle_{Si}$-oriented crystal. Rocking curves were recorded at Georgia Tech from both wafers (333_{Si} and $\bar{2}02_{Si}$ from the $[111]_{Si}$ and $[\bar{1}01]_{Si}$ wafers, respectively). Rocking curve full width at half-maximum (FWHM) and peak reflectivities (111_{Si} and 333_{Si}) were recorded at SSRL from the $[111]_{Si}$-oriented wafer and compared to results from a perfect Si crystal. Peak reflectivity and FWHM of 004_{Si} from a $[001]_{Si}$-oriented $TaSi_2$ wafer was also measured.

The FWHM of rocking curves was measured as a function of irradiated area at both Georgia Tech and SSRL; these FWHM measurements were made on the $[111]_{Si}$-oriented crystal using 333_{Si}. At Georgia Tech the mismatch between monochromator and sample *d* spacings produced dispersion of the $K\alpha_1$ and $K\alpha_2$ wavelengths, and in these measurements a narrow detector slit was used to eliminate the $K\alpha_2$ peak. A thin, slitlike lead mask was used to cover all but a narrow portion of the sample, and rocking curves were recorded with the mask in place. The dimensions of the area irradiated by $K\alpha_1$ without the mask were about 2.0×2.0 mm^2. With the mask present the dimension was unchanged along the direction normal to the incident beam and was first 1.0 mm and later 0.5 mm along the incident beam direction. At SSRL the FWHM at the 333_{Si} rocking curve was measured for irradiated areas ranging from 4×12 mm^2 to 0.4×1 mm^2.

Triple-axis diffractometry in the Bragg setting was performed at UCLA with a Bede Scientific D3 system and with a Cu x-ray tube. The first axis consisted of a channel cut 111_{Si} collimator (+, −) and a 111_{Si} monochromator (−). The sample was mounted on the second axis, and a channel cut 111_{Si} analyzer (+, −, +, −) was used. Double-axis scans of the $[111]_{Si}$-oriented wafer were recorded from 111_{Si}, 222_{Si}, and 333_{Si}. Reciprocal space maps were also recorded from 111_{Si} and 333_{Si} using a series of scans along $q_\perp$ (step size of 2 arcsec) with a separation between scans of 30 arcsec. Transformation from diffractometer to reciprocal space coordinates followed the convention of Iida and Kohra.[17]

Microradiographs were recorded of a several millimeter thick section of a ceramic multichip module in order to illustrate the gain in x-ray intensity obtained using $TaSi_2$–Si crystals as monochromators for synchrotron radiation. The composite sample and a perfect Si wafer were mounted side by side on a motorized goniometer and inclined so that $(111)_{Si}$ selected a wavelength, near that of the Mo *K* edge, providing adequate penetration of the sample. The motorized translator allowed rapid switching between the two monochromators without disturbing their alignment, and microradiographs were recorded with the film (Kodak SR-5). One set of exposures were recorded with using the $[111]_{Si}$ $TaSi_2$–Si crystal as the monochromator, and the second set of exposures was recorded with the dislocation-free [111] Si crystal. Constant film development times were used, and the difference in exposure times was taken to be an approximate measure of the increased intensity provided by the composite crystal compared to perfect Si.

RESULTS AND DISCUSSION

The $\theta/2\theta$ powder diffraction scans of the $[111]_{Si}$ wafer showed the 111_{Si}, 003_{TaSi_2}, and 006_{TaSi_2} diffraction peaks. As expected from the very small volume fraction of $TaSi_2$ phase present, the 111_{Si} peak was more than 50 times as intense as

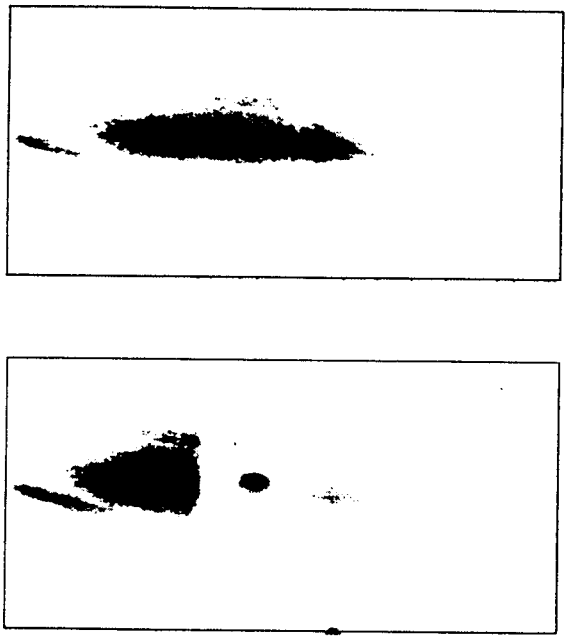

FIG. 3. Diffraction contrast from 003_{TaSi_2} with (bottom) and without (top) a 75-μm-thick Mo filter placed in the 1-mm-diam polychromatic beam.

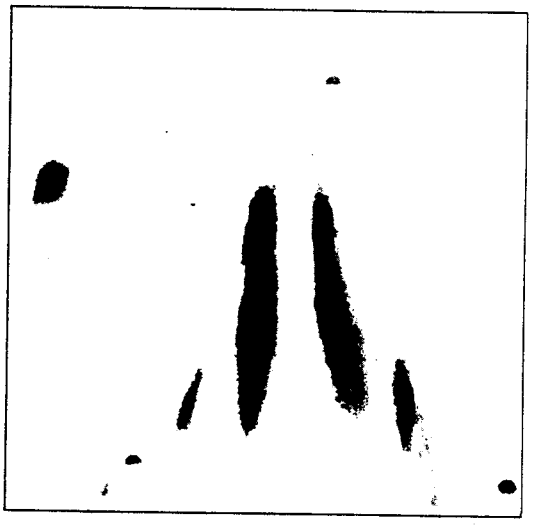

FIG. 4. Double streaks from 102_{TaSi_2} from the $[\bar{1}01]_{Si}$ wafer. The incident beam would be visible at the center of the upper edge of the image were the beam stop not in place.

either $00l_{TaSi_2}$ peak. The only other diffraction peak was the very weak 222_{Si}. Because 222_{Si} is structure factor forbidden, its presence indicates that significant strains are present in the matrix of the composite. The diffraction patterns from the $[\bar{1}01]_{Si}$ wafer revealed strong diffracted intensity from $\bar{2}02_{Si}$ and $\bar{4}04_{Si}$ and the following weak $TaSi_2$ reflections: 100, 200, 220, and 310. Note that all of the $TaSi_2$ reflections are from the $00l_{TaSi_2}$ zone; the fact that not all members of the zone are observed is not particularly troubling given the weakness of the reflections and the noise intrinsic to rapidly run, coarsely stepped scans such as those used here.

The earlier transmission synchrotron Laue patterns[11] revealed six streaks that were symmetrically arranged around the growth direction of the composite wafers (i.e., $[111]_{Si}$). Each streak was from a different $\{l00\}_{TaSi_2}$ (i.e., $\{l00\}_{TaSi_2}$ were perpendicular to $[111]_{Si}$), and the narrow azimuthal spread in each streak indicated a strong degree of preferred orientation between the silicide and matrix. Coupled with the strong texture in the $\theta/2\theta$ diffraction patterns, the earlier results and the known values of the $TaSi_2$ lattice constants[18] allow construction of the stereographic projection shown in Fig. 1. For simplicity the directions in the Si matrix are denoted by "*hkl*" while the normals to the $(mn.o)_{TaSi_2}$ are shown as "N_{mno}" for this hexagonal phase. Note that $[111]_{Si} \perp (001)_{TaSi_2}$, $[\bar{1}01]_{Si} \perp (100)_{TaSi_2}$ and $[012]_{Si}$ is within 1° of being normal to $(102)_{TaSi_2}$.

Figure 2, recorded with the Mo filter in the beam, shows the Laue pattern recorded from the $[\bar{1}01]_{Si}$ wafer oriented to diffract 003_{TaSi_2}. The 003 streak is labeled by "1," and the position of the beam stop is indicated by "○". Most of the streaks from the $TaSi_2$ rods appeared similar to the 003 reflections shown with an without the Mo filter in Fig. 3. With the filter present, a large change in contrast occurs for those rods diffracting wavelengths at the absorption edge of the filter material. The preferred orientation of $TaSi_2$ relative to the Si matrix is, however, somewhat more complex than was originally thought: Double streaks from 102_{TaSi_2} are seen in Fig. 4 from the longitudinally cut wafer (i.e., the $[\bar{1}01]_{Si}$ wafer), and there is an approximately 10°–15° azimuthal rotation between the two streaks. Reexamination of the Laue patterns recorded from the $[111]_{Si}$ wafer reveals a similar doubling of a few of the streaks; here the azimuthal rotation was 3° or 4°. It remains to be determined whether the angles measured between pairs of streaks are intrinsic to the crystallography of the $TaSi_2$–Si system or whether the two populations arise fortuitously as a response to the growth conditions, i.e., as a growth accident. Table I gives the experimentally measured Bragg angles (for the Mo *K*-edge wavelength) and corresponding *d* spacings for the streaks from the following reflections of the $TaSi_2$ rods: 003, 101, and 102. Note that results for 100_{TaSi_2} and 006_{TaSi_2} are not included in Table I as the former has been reported elsewhere[11] and the latter duplicates the information for 003.

The streaks for 003_{TaSi_2} and 102_{TaSi_2} were much more intense than those observed from 101_{TaSi_2} and 100_{TaSi_2} even allowing for the differences in exposure times and storage ring current. The relative intensities of the different streaks agree qualitatively with those given in the Powder Diffraction File[18] when one corrects for multiplicity[19] and for the fact that only about one-third of the area of the 1-mm-diam collimated beam reached the sample in the exposures of the

TABLE I. $TaSi_2$ experimental Bragg angles θ_B (for the Mo *K*-edge wavelength) and *d* spacings along with the assigned *hkl* and with expected *d* spacings d_{PDF} from the Powder Diffraction File (Ref. 18).

θ_B (deg)	*d* (Å)	Indices	d_{PDF} (Å)
5.07	3.51±0.15	101	3.504
6.99	2.55±0.02	102	2.573
8.21	2.17±0.015	003	2.190

TABLE II. Double-axis rocking curve full width at half-maximum (FWHM) and peak reflectivity for $TaSi_2$–Si compared to Si ($FWHM_{Si}$).

Reflection	FWHM (arcsec)	Peak reflectivity	$FWHM_{Si}$ (arcsec)
111	150	20%	7.4
333	58	8%	1.99
004	64.8	17%	3.6

101_{TaSi_2} streaks and about three-fourths of the beam area contributed to the images of the 102_{TaSi_2} streaks. The origin of the smaller beam areas for the 101_{TaSi_2} and 102_{TaSi_2} streaks was the relatively large rotations required to align 101_{TaSi_2} and 102_{TaSi_2} for diffraction: The lead shielding on the sample partially clipped the incident beam.

The range of orientations over which the 003_{TaSi_2} streak shows large diffracted intensity at the Mo K_{edge} wavelength was measured in 2° increments and definitely extended over 4° and possibly 1° farther in either direction. The range over which 100_{TaSi_2} diffracted was measured in 2.5° increments and extended over at least 5° and possibly 1° farther in either direction. These results, and the fact that the streaks are quite narrow laterally (about the width expected from the collimator diameter which demonstrates that the azimuthal angular range is quite small), demonstrate how highly oriented the rods are with respect to the matrix. Both of the double streaks from 102_{TaSi_2} were also quite narrow laterally.

Table II compares FWHM and peak reflectivity values for three Si reflections in $TaSi_2$–Si samples with values measured from perfect Si crystals. The values of FWHM for $TaSi_2$–Si were approximately 20 times greater than those for perfect Si, but the reflectivity decreased by a factor of about 4. It is interesting to note that $\bar{2}02_{Si}$ rocking curves from the $[\bar{1}01]_{Si}$ wafer showed different FWHM values depending on whether the sample was rotated about $[111]_{Si}$ or $[1\bar{2}1]_{Si}$: 206 arcsec versus 63 arcsec, respectively. The very real possibility exists, therefore, of tuning to a desired bandpass without changing the diffracting planes.

The different $\bar{2}02_{Si}$ rocking curve widths suggest that the curvature of $(\bar{1}01)_{Si}$ about an axis parallel to the rods (i.e., $[111]_{Si}$) is considerably greater than the curvature of $(\bar{1}01)_{Si}$ about an axis normal to the rods (i.e., $[1\bar{2}1]_{Si}$). This corresponds to the reciprocal lattice points having significantly different dimensions along the different crystallographic directions. The large difference of thermal expansion coefficients [8.8–10.7 ppm/°C for $TaSi_2$ compared to 3 ppm/°C for Si (Ref. 20)] will produce considerable strain during cooling from the eutectic temperature of 1385 °C,[21] and one would expect a matrix containing an array of parallel of rods would respond anisotropically to the resulting thermal stresses.

Representative polychromatic reflection topographs recorded from the $[\bar{1}01]_{Si}$ wafer are shown in Fig. 5. Figure 5(a) shows a $\bar{2}02_{Si}$ topograph recorded with the incident beam direction coplanar with $[111]_{Si}$ and Fig. 5(b) shows a second topograph recorded with the incident beam parallel to $[1\bar{2}1]_{Si}$. Both topographs in Fig. 5 were recorded with a wavelength of approximately 1.5 Å. Light and dark bands are visible along the wafers' growth direction, i.e., along

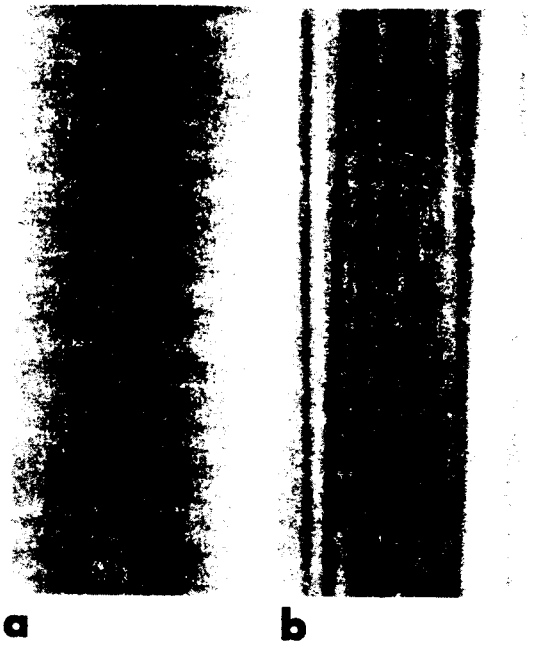

FIG. 5. Polychromatic reflection topographs of the $[\bar{1}01]_{Si}$ wafer recorded with ~1.4 Å radiation. (a) $\bar{2}02_{Si}$ topograph recorded with the incident beam coplanar with $[111]_{Si}$. (b) $\bar{2}02_{Si}$ topograph recorded with the incident beam at 90° to that in (a), i.e., coplanar with $[1\bar{2}1]_{Si}$. The field of view in the vertical direction is 14.0 mm. In both cases the projection of the incident and diffracted beams are horizontal.

$[111]_{Si}$, the direction of the rods' axes. In Fig. 5(a) there seem to be finer gradations in the bands than in Fig. 5(b) and there are small circular features diffracting little intensity in Fig. 5(a) and not in 5(b). The anisotropic distribution of diffracted intensity in the reflection topographs is consistent with the observations in the preceding paragraphs, that is, of differing rocking curve FWHMs for the same diffraction vector but different rotation axes.

Rocking curves ($K\alpha_1$, 333_{Si} from the $[111]_{Si}$ wafer) recorded at Georgia Tech with 2.0, 1.0, and 0.5 mm mask openings produced FWHM values of 86, 85, and 76 arcsec, respectively. The FWHM of 333_{Si} measured on the SSRL laboratory double-axis system changed from 79 to 59 arcsec upon reducing the area irradiated from 4×12 mm^2 to 0.4×1

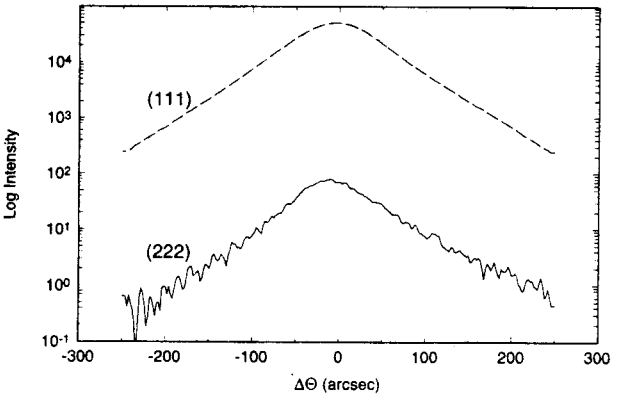

FIG. 6. Double-axis rocking curves superimposing the 111_{Si} (centered at a Bragg angle of 14.112°) and the structure factor forbidden 222_{Si} (centered at a Bragg angle of 29.426°) reflections from the $[111]_{Si}$ wafer.

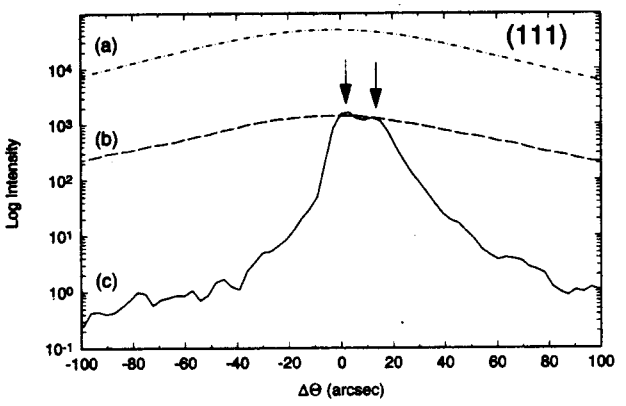

FIG. 7. Comparison of diffraction scans for 111_{Si} using double- and triple-axis measurements for the $[111]_{Si}$ wafer. (a) Double-axis rocking curve showing the large FWHM. (b) Triple-axis ω scan (along q_y in the reciprocal space maps) with FWHM similar to that in the double-axis measurement. (c) Triple-axis $\theta/2\theta$ measurement showing a much lower FWHM and the presence of strain in the crystal (arrows).

mm^2. The relatively small change in FWHM with a fairly large change in area irradiated indicates that long-range curvature is not the origin of the large rocking curve widths observed in the $TaSi_2$–Si wafers.

Measurements of the $[111]_{Si}$ wafer with the triple-axis diffractometer present a picture similar to that described above and add considerably to the understanding of the strains and mosaic in the $TaSi_2$–Si system. Double axis rocking curves of 111_{Si} and the structure-factor forbidden 222_{Si} are shown in Fig. 6 Note that 111_{Si} and 222_{Si} are centered at Bragg angles of 14.112° and 29.426°, respectively; the curves are superimposed on the same angular scale for ease of comparison. The FWHM of 111_{Si} is about 93 arcsec while that of 222_{Si} is 77 arcsec. Figure 7 compared 111_{Si} diffraction scans using double- and triple-axis modes [curves (a)–(c) show the double-axis rocking curve, the triple axis ω scan, i.e., a scan along q_y in the reciprocal space map in Fig. 9, and the triple axis $\theta/2\theta$ scan, respectively]. Note that the double-axis rocking curve and the triple-axis ω scan have similar widths while the $\theta/2\theta$ curve is much narrower and appears to have two maxima. Figure 8 shows the triple-axis ω scan and $\theta/2\theta$ scans for 333_{Si}; as would be expected in a

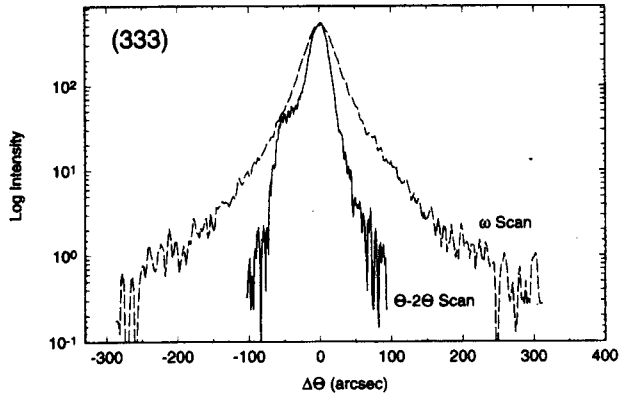

FIG. 8. Triple-axis ω and $\theta/2\theta$ scans for 333_{Si} from the $[111]_{Si}$ wafer.

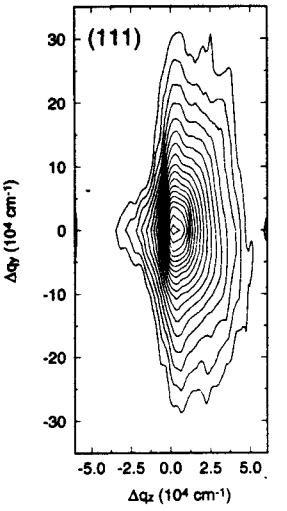

FIG. 9. The 111_{Si} reciprocal space map from the $[111]_{Si}$ wafer. The origin of reciprocal space is along the horizonal direction. The vertical axis of each plot, Δq_y, represents mosaic and is often labeled as $q_\parallel$, and the horizontal axis, Δq_z, shows lattice parameter changes and is often labeled $q_\perp$. Variations in lattice tilt represent the primary contribution to the large FWHM observed in double-axis measurements.

situation where mosaic and microstrain broadening were present, the pair of 333_{Si} scans have more comparable FWHM than the corresponding 111_{Si} scans.

The 111_{Si} and 333_{Si} reciprocal space maps of the $[111]_{Si}$ wafer are shown in Fig. 9 and 10, respectively. The vertical axis of each plot, Δq_y, represents mosaic and is often labeled as $q_\parallel$, and the horizontal axis, Δq_z, shows lattice parameter changes and is often labeled $q_\perp$. Variation in lattice tilt, that is, mosaic, represents the primary contribution to the high FWHM observed in the double-axis measurements. Microstrain also contributes to the double-axis FWHM, but this contribution is not as important as that of the mosaic. Note that in these figures the origin of reciprocal space is along the

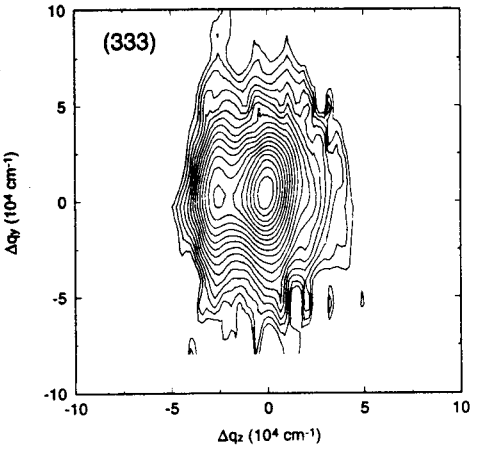

FIG. 10. The 333_{Si} reciprocal space map from the $[111]_{Si}$ wafer showing the Si matrix is under strain due to the presence of the $TaSi_2$ rods. The vertical axis of each plot, Δq_y, represents mosaic and is often labeled as $q_\parallel$, and the horizontal axis, Δq_z, shows lattice parameter changes and is often labeled $q_\perp$. The origin of the plot is shifted 66 arcsec from the peak position of perfect Si.

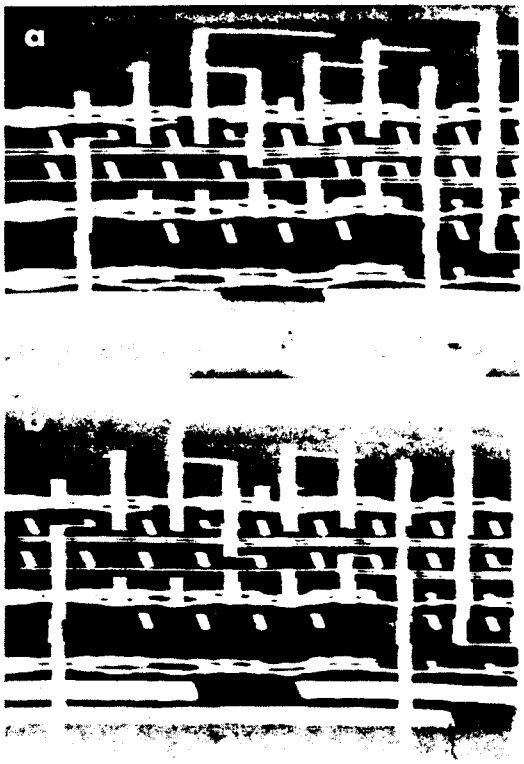

FIG. 11. Microradiographs recorded of a section of a ceramic multichip module showing contrast from the metal tracks and vias within the sample. In (a) monochromatic radiation from a perfect Si crystal was used while in (b) the $[111]_{Si}$ $TaSi_2$–Si wafer was used as the monochromator. The lighter regions represent decreased transmitted intensity. The field of view in the horizontal direction is 4.5 mm.

horizontal direction and that variations in lattice tilt or mosaic are along the vertical axis (i.e., along Δq_y). The origin of the maps of the 111_{Si} and 333_{Si} reciprocal lattice points are set at the position of the highest diffracted intensity. The origin of the 333_{Si} reciprocal lattice point of the composite was shifted to an angle 66 arcsec higher than that of a perfect Si reference crystal; this corresponds to a compressive strain of 3×10^{-4} for the Si matrix of the composite relative to the reference Si crystal. The origin of the double peaks, particularly visible in the 333_{Si} reciprocal space map, is at present obscure; the peaks may represent the effect of polishing damage and/or surface relaxation or may represent the effect of significant compressive strain gradients in the Si matrix. The results of triple-axis diffractometry are consistent with the double-axis measurements which indirectly indicate that long-range lattice bending is not the dominant contribution to the large FWHM. These results, therefore, support the conclusion that the $TaSi_2$–Si wafers can provide a suitably broad bandpass for synchrotron experiments requiring the highest possible fluxes and not needing high-energy resolution. Use of the $[111]_{Si}$ $TaSi_2$–Si wafer as an analyzer crystal for double-axis diffractometry using a polychromatic beam incident on the sample crystal is described elsewhere.[16] The increased intensity obtained when using the composite crystal as a monochromator instead of a perfect Si crystal is demonstrated by the microradiography results which follow.

Microradiographs of a section of a ceramic multichip module are shown in Fig. 11(a) using monochromatic radiation from a (111) Si crystal and 11(b) using radiation from the $[111]_{Si}$ $TaSi_2$–Si wafer. The field of view in the horizontal direction is 4.5 mm, and the exposure times for (a) and (b) were 5 and 50 s, respectively, at beam currents of between 57 and 58 mA. There seems to be little difference in image quality between the two microradiographs. Perhaps the separations between the three closely spaced, parallel tracks (two sets running horizontally from the middle right-hand side of the images) are marginally better defined in (a) than in (b), but this could be due to vagaries of processing the original microradiographs or of printing the images. The two emulsions have very nearly equal optical density, meaning that the total flux incident on each was nearly the same, and the gain in speed of at least a factor of 10 could be important in dynamic radiographic experiments requiring imaging with monochromatic radiation for contrast resolution.

Gains of an order of magnitude in intensity are also important for microbeam applications: When one employs micrometer- or submicrometer-sized probes, even at the current generation of synchrotron radiation sources (e.g., APS and ESRF), one is operating in a photon-starved mode. Focusing optics are typically used to deliver more photons to the area or volume of interest, and combining bending with the use of $TaSi_2$–Si wafers would seem to offer a major improvement over current capabilities.

CONCLUSIONS

The data presented show that $TaSi_2$–Si *in situ* eutectic composites are suitable for use as high-flux, wide-bandpass monochromators for synchrotron radiation applications not requiring high-energy resolution. Diffraction from the $TaSi_2$ rods produces streaks in synchrotron Laue patterns, shows the relative orientations of Si and $TaSi_2$ phases and demonstrates that the spread of rod orientations is less than 6° [i.e., $(001)_{TaSi_2}$ is no more than 3° misoriented from being parallel with $(111)_{Si}$]. Double-axis diffractometry with 8 keV x rays reveals very wide rocking curves accompanied by appreciable peak reflectivities, and this is shown to be the combined result of "micro"- or short-range mosaicity and microstrain, and not macroscopic bending of the crystal.

ACKNOWLEDGMENTS

The work reported herein was partially done at SSRL which is supported by the Department of Energy, Office of Basic Energy Sciences; and the National Institutes of Health, Biotechnology Resource Program, Division of Research Resources. The authors thank Dr. Quang V. Nguyen and Philip G. Rossoni of SME Technologies (21 Davis Rd., Belmont, MA 02178) for providing the $[\bar{1}01]_{Si}$ wafer and Dr. Brian M. Ditchek, formerly of GTE Laboratories, for providing the $[111]_{Si}$ wafer. The authors thank A. Guvenilir, D. P. Piotrowski, and J. D. Haase of the School of Materials Science and Engineering, Georgia Institute of Technology, for helping to collect some of the synchrotron Laue patterns.

[1] A. Muller and M. Wilhelm, J. Phys. Chem. Solids **26**, 2021 (1965).
[2] B. Reiss and T. Renner, Z. Naturforsch A **21**, 546 (1966).
[3] L. M. Levinson, Appl. Phys. Lett. **21**, 289 (1971).

[4]N. J. Helbren and S. E. R. Hiscocks, J. Mater. Sci. **8**, 1744 (1973).
[5]D. E. Holmes, J. Electrochem. Soc. **128**, 859 (1981).
[6]B. M. Ditchek, J. Appl. Phys. **57**, 1967 (1985).
[7]B. M. Ditchek, J. Cryst. Growth **75**, 264 (1986).
[8]B. M. Ditchek, B. G. Yacobi, and M. Levinson, Appl. Phys. Lett. **51**, 267 (1987).
[9]B. M. Ditchek and M. Levinson, Appl. Phys. Lett. **49**, 1656 (1986).
[10]B. G. Yacobi and B. M. Ditchek, Appl. Phys. Lett. **50**, 1083 (1987).
[11]S. R. Stock, Z. U. Rek, Y. H. Chung, P. C. Huang, and B. M. Ditchek, J. Appl. Phys. **73**, 1737 (1993).
[12]A. Freund, Proc. SPIE **1740**, 58 (1992).
[13]H. Shiwaku, K. Hyodo, and M. Ando, Jpn. J. Appl. Phys. **30**, 2065 (1991).
[14]P. Zaumseil, U. Winter, S. Joksch, and A. Freund, Rev. Sci. Instrum. **63**, 907 (1992).
[15]B. G. Yacobi and B. M. Ditchek, in *Microscopy of Semiconductor Materials*, edited by A. G. Cullis and P. D. Augustus, Institute of Physics Conference Series 87 (IOP, Bristol, 1987), Sec. 11, p. 703.
[16]S. R. Stock, A. Guvenilir, D. P. Piotrowski, and Z. U. Rek, in *Applications of Synchrotron Radiation Techniques to Materials Science II*, Mater. Res. Soc. Proc. Vol. 375 (MRS, Pittsburgh, PA, 1995), p. 275.
[17]A. Iida and K. Kohra, Phys. Status Solidi A **51**, 533 (1979).
[18]Card 38-483, Powder Diffraction File, Joint Committee for Powder Diffraction Standards, International Centre for Diffraction Data.
[19]B. D. Cullity, *Elements of X-ray Diffraction*, 2 ed. (Addison–Wesley, Reading, MA, 1978), Appendix 13.
[20]S. P. Murarka, *Silicides for VLSI Application* (Academic, New York, 1983).
[21]M. Hansen, *Constitution of Binary Alloys*, 2nd ed. (McGraw–Hill, New York, 1958).